REPORT VOLCANICA

Report on the lava flow daily monitoring of the 19 September–05 October 2022 eruption at Piton de la Fournaise

Magdalena Oryaëlle Chevrel*[α,β,γ], Nicolas Villeneuve[β,γ,δ], Raphaël Grandin[γ], Jean-Luc Froger[ε], Diego Coppola[ζ], Francesco Massimetti[ζ], Adele Campus[ζ], Alexis Hrysiewicz[η,θ], and Aline Peltier[β,γ]

[α] Université Clermont Auvergne, CNRS, IRD, OPGC, Laboratoire Magmas et Volcans, 63000 Clermont-Ferrand, France.
[β] Observatoire Volcanologique du Piton de la Fournaise, Institut de Physique du Globe de Paris, 97418 La Plaine des Cafres, France.
[γ] Université Paris Cité, Institut de Physique du Globe de Paris, CNRS, 75005 Paris, France.
[δ] Université de La Réunion, Laboratoire GéoSciences Réunion, 97744 Saint Denis, France.
[ε] Université Jean Monnet - Faculté des Sciences et Techniques, Laboratoire de Géologie de Lyon : Terre, Planètes, Environnement - UMR CNRS 5276, France.
[ζ] Dipartimento di Scienze della Terra, Universita degli Studi di Torino, Torino, Italy.
[η] SFI Research Centre in Applied Geosciences (iCRAG), University College Dublin, Belfield, Dublin 4, Ireland.
[θ] UCD School of Earth Sciences, University College Dublin, Belfield, Dublin 4, Ireland.

Abstract

Taking prompt and effective actions to mitigate risks associated with an effusive eruption greatly depends on the monitoring of lava flow emplacement. Here we report on the monitoring of the lava flow emplaced during the 19 September to 05 October 2022 eruption at Piton de la Fournaise (La Réunion) that involves an unprecedentedly large data set acquired using multiple techniques and sensors. These include aerial photogrammetry to construct digital surface models and define lava flow geometry during and after emplacement. Complementary use of multiple satellite sensors (visible, infrared and radar) allowed lava flow field contour definition and an estimation of time-averaged discharge rate with daily frequency. Evolution of the eruptive cone morphology was also monitored through aerial photogrammetry and radar multi-viewing angle imagery. This combination of data obtained from several institutes and using various techniques—from ground, air and space—allowed detailed tracking of lava flow advance and serves as an example for future eruptions at Piton de La Fournaise and at other active volcanic sites.

Résumé

Prendre des mesures rapides et efficaces pour atténuer les risques associés à une éruption effusive dépend grandement du suivi de la mise en place de la coulée de lave associée. Nous reportons ici les détails de la surveillance de la coulée de lave mise en place lors de l'éruption du 19 septembre au 5 octobre 2022 au Piton de la Fournaise (La Réunion) impliquant l'acquisition quotidienne d'informations inédites sur la coulée de lave à partir de plusieurs techniques et capteurs. Ces informations incluent de la photogrammétrie aérienne pour construire des modèles numériques de surface et définir la géométrie de la coulée de lave pendant et après sa mise en place. Des acquisitions quotidiennes d'images satellites (dans le visible, infrarouge et radar) ont permis également de tracer les contours de la coulée et d'estimer un taux d'effusion moyenné dans le temps, ainsi que le volume de lave émis. La combinaison de données provenant de plusieurs instituts et utilisant diverses techniques – depuis le sol, les airs et l'espace – a permis un suivi détaillé de l'avancée des coulées de lave, servant ainsi d'exemple pour de futures éruptions au Piton de La Fournaise et sur d'autres sites volcaniques actifs.

Keywords: Lava flow; Basaltic volcano; Effusive eruption; Monitoring; Remote sensing; La Réunion.

1 Introduction

Piton de la Fournaise (La Réunion Island) is an active basaltic hotspot volcano that produces mainly effusive eruptions associated with lava fountains and the emission of lava flows. Since 1998, eruption frequency has been on average twice a year. Rarely, phreatic and phreatomagmatic eruptions have occurred in the past with a centennial recurrence [Michon et al. 2013]. For at least the last hundred years, eruptive activity at Piton de la Fournaise has been controlled by cycles related to magma source and to stress field [Peltier et al. 2009; Got et al. 2013; Vlastélic et al. 2018; Derrien 2019]. In 2014, after 4 years of quiescence, Piton de la Fournaise entered a new cycle and between then and now (June 2023) it has erupted 24 times (Figure 1). These eruptions lasted between 0.5 and 50 days and produced between 0.3 and 35 Mm^3 of lava. The common eruptive dynamic consists of the construction of an eruptive cone by lava fountaining and lava flows reaching distances of up to 3 km on average [Chevrel et al. 2021]. Lava flows are mostly channelized 'a'ā flow type with sometimes the development of tube systems and pāhoehoe breakouts.

At the end of 1979, the *Observatoire volcanologique du Piton de la Fournaise* at the *Institut de physique du globe de Paris* (OVPF-IPGP) was created to monitor Piton de la Fournaise. Monitoring includes local (on-site ground or aerial) and distal (satellite) data acquisitions by OVPF-IPGP, and by its partners from SNOV (*Service national d'observation en volcanologie*) at IPGP and OPGC (*Observatoire de physique du globe de Clermont Ferrand*), and from foreign agencies (e.g.

* oryaelle.chevrel@ird.fr

Submitted: 2022-12-05 | Accepted: 2023-08-15 | Published: 2023-10-26
Editor: A. Whittington | Typesetter: E. Hughes

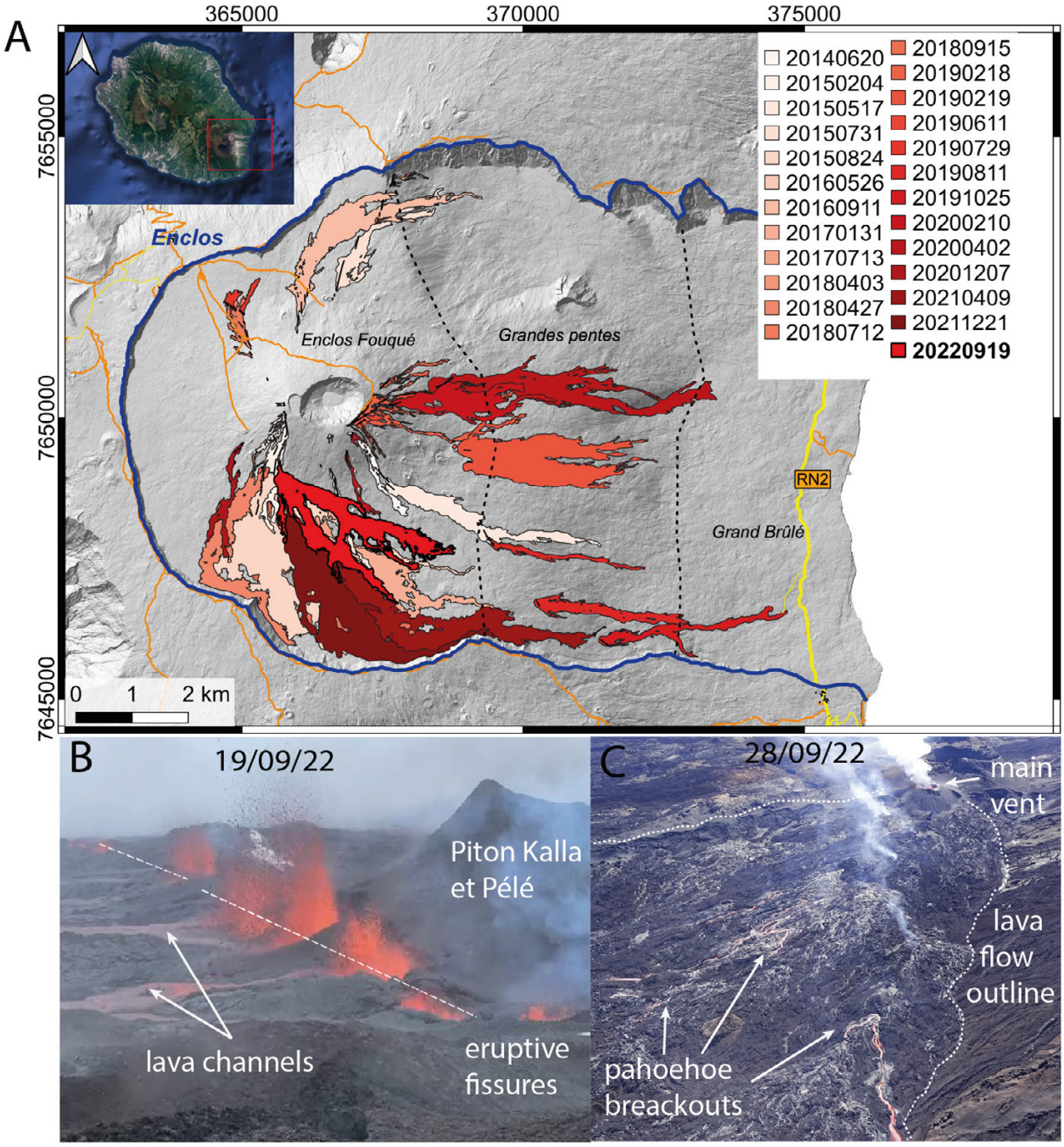

Figure 1: Location of the eruption. [A] Lava flows (color coded) from 2014 to end of 2022 (legend indicates the eruption starting date: YYYYMMDD). The limits of the *Enclos* (including caldera and collapse structures) is shown by the blue line. The background is a 1-m resolution hill-shaded reference DSM (coordinates are given in meters within system WGS84-UTM 40S). Road (yellow line) and trails (orange lines) are from 2020 BD TOPO® IGN. The dashed black lines divide the *Enclos* into three main domains: *Enclos Fouqué Caldera*, *Grandes Pentes*, and *Grand Brûlé*. [B] Photograph of the fissure on the first day of the eruption showing the eruptive fissure and incipient lava channel. For scale, the height of an older scoria cone on the background (*Piton Kalla et Pélé*) is 25 m. Photo credit to PGHM (*Pelotons de gendarmerie de haute montagne*). [C] Aerial photograph of the proximal area of the lava flow field taken on 28 September, showing the main vent and the multiples active breakouts of pāhoehoe lava. The distance between the main vent and the bottom of the picture is about 600 m. Photo credit to OVPF.

University of Turin, Italy). The dense monitoring network at Piton de la Fournaise, and expertise at OVPF-IPGP and its partners, has been therefore highly efficient at responding to effusive eruptions [Roult et al. 2012; Bato et al. 2016; Staudacher et al. 2016; Harris et al. 2017; Peltier et al. 2018; Harris et al. 2019; Peltier et al. 2021; Chevrel et al. 2022; Peltier et al. 2022]. In parallel, a complete database of lava flow outlines since 1930 has been compiled using various techniques and includes, to date, more than 200 lava flows [Bachèlery 1981; Servadio 2011; Servadio et al. 2012; Derrien 2019; Derrien et

al. 2019; Chevrel et al. 2021]. Since the first eruption monitored by OVPF-IPGP in February 1981, lava flows have been systematically mapped at the end of each eruption. Until 2010, mapping was done by hand-held GPS and from aerial photographs taken onboard ultralight aircraft. Aerial photography acquisition campaigns to perform Structure-from-Motion Multi-View Stereo (SfM-MVS) photogrammetry were specifically carried out to study lava flows for the first time in 1998 and 2007.

Since 2014, recurrent aerial surveys (from helicopter or ultra-light motorized planes, ULM) produced for SfM-MVS photogrammetry have been systematically done at the end of each eruption of Piton de la Fournaise and sometimes during the eruption (when the weather conditions and the timing of the eruption allow) to monitor the evolution of the flow field and to calculate the thickness and volume of the emitted lava flow [Derrien 2019; Derrien et al. 2019]. Additionally, punctual Unoccupied Aerial Systems (UAS) surveys are also often conducted, although not routinely. Satellite data such as InSAR (satellite-based Interferometry of Synthetic Aperture Radar) coherence maps, Pléiades, ASTER and Sentinel-2 images have also been used to delimit lava flow coverage [Bato et al. 2016; Harris et al. 2017; 2019]. Furthermore, the monitoring and forecasting of lava flows at Piton de la Fournaise have been enhanced over the past years with the near real-time response protocol that has been systematically employed since 2018, providing lava flow hazard maps to the authorities within the first hours of the eruption [Chevrel et al. 2022].

In this report, we aim at presenting the lava flow monitoring of the 19 September to 05 October 2022 eruption of Piton de la Fournaise, which is remarkably detailed. Indeed, we collected more than 20 satellite images and 4 series of aerial images during the eruption. We were able to define 18 outlines at a rate of 1–3 outlines per day during the 16 days of the eruption. The aerial images were obtained for SfM analyses via UAS and ULM surveys. Satellite images include InSAR coherence maps, Sentinel-2 images and, for the first time at Piton de la Fournaise, PlanetScope images. The eruptive cone morphology was also tracked through SfM and multi-angle radar imagery via Capella Space products. As a complement, thermal satellite images were also collected to derive time-averaged discharge rate (TADR) and cumulative lava volume as usually obtained when using satellite-data-driven platforms. Collectively, this represents an unprecedentedly detailed lava flow tracking at Piton de la Fournaise that was achieved mainly thanks to good weather conditions but also thanks to efforts to combine various techniques from different institutes. Here, we aim at showing that working in synergy with various sensors ensures detailed lava flow tracking that is necessary to implement lava flow emplacement models and enhances rapid and efficient response to eruption monitoring.

2 Overview of the 19 September–5 October 2022 eruption

On 19 September 2022, at 6:23 Réunion Time (RET = UTC+4), an earthquake swarm was recorded, signaling the rupture of the roof of the shallow magma reservoir and the propagation of magma towards the surface. Surface displacements, recorded by GNSS method and InSAR, reached up to 40–50 cm on the southern flank of the volcano [OVPF 2022]. The eruptive tremor, caused by the arrival of magma close to the surface, marked the onset of the eruption at around 7:48 RET. Eruptive fissures opened over a distance of 380 m, at the foot of the scoria cone formed during the August 2015 eruption (*Piton Kalla et Pélé*). The first hours of the eruption were characterized by lava fountaining and the emission of lava flowing eastward. Near the fissure, the lava flow field was composed of multiple incipient channels of a few meters wide, and pāhoehoe overflows (Figure 1B). Around 400 m from the eruptive fissures, the lava flow field developed three main ʻaʻā branches, between 100 and 200 m wide, that reached a distance of 2.4 km within the first hours. By the end of the first day, activity was concentrated at a single vent at about 2200 m above sea level (a.s.l). At that time the longest branch of the lava flow had reached 1890 m a.s.l.

From the second day and over the following ten days, the eruptive activity remained stable with weak lava fountaining that constructed a scoria cone (that would later be named *Piton Tikal*). The effusive activity took place mainly through lava tubes with multiple small lava breakouts throughout the lava field, forming small ephemeral channels of a couple of meters wide and areas covered with pāhoehoe slabs and lobes (Figure 1C). The lava flow field did not significantly expand.

On 29 September at around 21:40 RET, the amplitude of the eruptive tremor increased and was accompanied by an intensification of lava fountaining and lava flow expansion. Lava flow expansion was fed by tube systems and channels and concentrated to the front. The northern lava flow front advanced a few hundred meters and new branches developed to the south (see Section 4.1). The increased fountain activity provoked a significant morphology change of the eruptive cone and subsequent growth (see Section 4.2). The eruptive activity remained similar for another six days.

The eruption was declared finished on 05 October 2022 around 10:10 RET based on a sudden stop of the eruptive tremor and no more lava emission on the surface. Although a new weak tremor was recorded on 06 October (11:40 RET) to 07 October (15:00 RET), and expulsion of very small quantity of remnant magma from the conduit was observed within the cone on 06 October between 18:30 and 19:30 RET, the end of the eruption was officially registered by the observatory to 05 October 2022 at 10:10 RET.

3 Methods and data collections

3.1 Structure from Motion photogrammetry using aerial photographs

Both UAS and classical (occupied) ultralight aircraft were employed to perform SfM photogrammetry and produce georeferenced digital surface models (DSM) and orthomosaics of the flow field [e.g. James et al. 2020]. DSM and orthomosaics were obtained for syn- and post-lava flow emplacement following the method presented in previous studies at Piton de La Fournaise [Derrien 2019; Derrien et al. 2019; 2020]. This method consists of generating point clouds from the acquired aerial images using `Metashape Pro` (v1.8.4) and comparing them

using CloudCompare to obtain the outline, thickness and volume of the lava flow.

During this eruption, two UAS surveys were carried out to cover the vent area. For this, the DJI mini UAS (equipped with a 12 MPix FC7203 camera) was used on 28 September and the DJI Mavic 3 UAS (with a 20 MPix L1D-20C camera) was used on 03 October. Images were acquired in oblique view and covered a circle of 90 m in radius centered on the main vent and in vertical view (at heights of 78 m and 191 m for the two acquisitions, respectively). The error in the coordinates (due to the accuracy of the GNSS receiver and the UAS motion) resulted in an Absolute Mean Shift (AMS) of 2.81 m and 2.92 m, respectively, in the horizontal direction. These two surveys allowed us to produce DSMs with 5.8 cm/pixel and 8.8 cm/pixel resolution, respectively. All details on the point clouds and the quality and accuracy of the DSM model are given in Supplementary Material Table S1.

Two ULM surveys were also carried out to cover the entire flow field, one on 24 September and the other on 05 October. Photographs were acquired manually using a Canon Mark III 5DSR camera (50 MPix) with an 85 mm lens at vertical and oblique views (angle <30°) at average heights of 752 m and 1100 m above the flow, respectively. Each photograph was associated with an Exif file that included the coordinates and height above the ellipsoid obtained via the Canon GPS receiver module (GP-E2) plug onto flash hot-shoe. The error on the coordinates (due to the GPS receiver accuracy and the aircraft motion) generated an AMS of 19 m and 24 m, respectively. The point cloud reprojection error is 0.7 pixels and 0.6 pixels, respectively. The produced DSMs from these two surveys have resolution of 8.51 cm/pixel and 12.9 cm/pixel, respectively. All details on the point clouds and the quality and accuracy of the DSM model are provided in Supplementary Material Table S1.

To correct for the shift and to compare the produced models (acquired both with UAS and ULM) with each other and with the pre-emplacement DSM, all point cloud models (pre-, syn- and post-emplacement) were resampled at 1 m using CloudCompare. To ensure comparison, models are also co-referenced to a reference point cloud (i.e. the reference DSM) using between 15 and 35 control points. In the present case, the reference DSM was produced using the SfM technique developed by Rupnik et al. [2016, 2018] applied to tri-stereoscopic from Pleiades* images acquired on 21 July 2021. The computation of the reference point cloud model and DSM were performed on the webservice "DSM-OPT" developed by ForM@Ter, the Solid Earth component of the Data Terra Research Infrastructure†. The reference DSM is also resampled at 1 m/pixel. This reference DSM was modified to include the lava field of the December 2021 eruption that occurred in the same area. The modification was done by adding the local DSM of the December 2021 lava flow, which was made through post-emplacement aerial SfM photogrammetry and following the same method as described here.

The re-sampling and co-referencing ensured that all models can now be correctly positioned and compared. The subtraction of the syn- and post-emplacement lava flow models to the reference model generated a thickness point cloud model (Supplementary Material Figure S1) that is used to calculate the volume of the emitted lava. The produced DSMs are then employed to orthorectify the mosaic and the produced orthomosaics are used to manually define the contours of the flows and kipukas using QGIS.

3.2 High-resolution optical imagery from PlanetScope constellation

For the first time at Piton de La Fournaise, we used high-resolution optical imagery acquired by commercial CubeSats "SuperDove" of the PlanetScope constellation‡. The constellation consists of >100 nanosatellites orbiting sun-synchronously at 500 km altitude, acquiring images at around 10:00 RET. Imagery was acquired by a frame camera with nadir viewing geometry, resampled at 3 m. The optical system is sensitive to 8 spectral bands, including 7 visible bands in the 431–713 nm range, and 1 Near Infrared (NIR) band spanning the 845–885 nm range§. Products are delivered to users ~24 hours after acquisition. We ordered images processed at the "surface reflectance" level, which incorporates geometric and radiometric corrections (orthorectification and atmospheric transmission) [Tu et al. 2022].

To highlight the outline of lava flows and facilitate lava flow mapping, we built three different combinations of SuperDove spectral bands (Figure 2):

- A false-color RGB composition using bands R=8 (NIR, 865 nm), G=4 (green, 565 nm) and B=2 (blue, 490 nm).
- A normalized difference vegetation index (NDVI) [Rouse Jr et al. 1974] using bands 6 (red, 665 nm) and 8 (NIR, 865 nm): $(R_{NIR} - R_{red})/(R_{NIR} + R_{red})$
- A red-edge triangular vegetation index (RTVI) [Chen et al. 2010] using bands 4 (green, 565 nm), 7 (red-edge, 705 nm) and 8 (NIR, 865 nm): $100(R_{NIR} - R_{red\text{-}edge}) - 10(R_{NIR} - R_{green})$.

Thanks to the glowing near-infrared radiation of the active lava flow, the NDVI and RTVI indexes provide clear contrasts across the lava flow borders. In total, we analyzed 9 cloud-free images during the course of the eruption (24, 26, 27, 29 September and 01, 02, 03, 04, 05 October), among which 7 were used to extract outlines (see example in Figure 2). The lava flow outlines were defined by hand on QGIS following the color contrasts on the georeferenced images.

3.3 InSAR (Interferometry Synthetic Aperture Radar)

Since the early 2000s, InSAR images are regularly acquired on Piton de la Fournaise in the framework of the Indian Ocean

*ESA data delivered by CNES as part of the Kalidéos program via the web service developed by ForM@Ter Solid Earth component of the Data Terra Research Infrastructure. This is part of a project supported by the DINAMIS program (funding from CNES, CNRS, IGN, IRD, INRAE, CIRAD).

†https://www.poleterresolide.fr/le-service-dsm-opt/

‡Data were delivered at no cost to the scientific partners of OVPF within the framework of "Education and Research Program" https://www.planet.com/markets/education-and-research/.

§https://assets.planet.com/docs/Planet_Combined_Imagery_Product_Specs_letter_screen.pdf

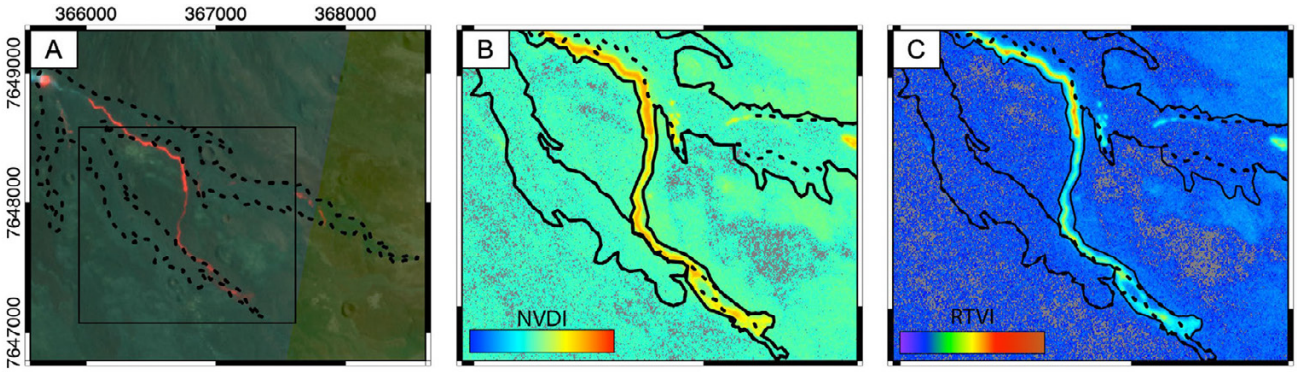

Figure 2: Example of PlanetScope images acquired on 2 October 2022 at 05:31 UTC in [A] false-color RGB bands, [B] normalized difference vegetation index (NVDI) and [C] red-edge triangular vegetation index (RTVI). Indices color scale (cold to warm) of NDVI or RTVI reflect thermal radiation intensity emitted by active lava flows. The dotted line represents the outline from the previous day and the continuous black line (in B and C) represents the updated lava flow outline that could be obtained from this acquisition. The rectangle in A bounds the images in B and C. Coordinates are in meters within system WGS-UTM 40S.

InSAR Observatory [OI2, Richter and Froger 2020]. If the radar backscattering properties of the ground change critically between two radar image acquisitions (e.g. due to the addition of new lava), there is a high InSAR coherence contrast between the area covered by the newly emplaced lava and the surrounding preserved area. The possibility to use such coherence contrast to map lava flows has been proved as an effective tool in several previous studies [Dietterich et al. 2012; Bato et al. 2016; Harris et al. 2019; Hrysiewicz 2019; Poland 2022].

During the studied eruption, 1 Stripmap Sentinel-1 (S1) (C-Band) and 7 Spotlight ALOS-2 (L-Band) images were acquired using different acquisition geometries, offering about 1 image every 2 days. All the SAR images were obtained for free, and the ALOS-2 from JAXA in the framework of an EO-ERA3 project. Combined with images taken in the same acquisition geometry in the days preceding the eruption, they were used to produce eight independent interferograms and coherence images (see Supplementary Material Table S2 and Figure S2). Both S1 and ALOS-2 images were processed using `DIAPASON` using the two-pass method described by Massonnet and Feigl [1998]. The topographic contribution was accounted for and removed from the interferograms using a 5-m resolution reference DSM produced by the French Geographic Institute (IGN) via lidar in 2008–2009. The same DSM was used for the interferometric product georeferencing, so the coherence images used to delineate the lava flow contour also have a 5-m resolution. Following the highly incoherent areas, the lava flow outlines were defined by hand on `QGIS` (Supplementary Material Figure S2), with the exception of the final lava flow outline from 05 October that was obtained through a semi-automatic procedure that detected the coherence contrast [Hrysiewicz 2019].

3.4 Capella images

For the first time at Piton de la Fournaise, Cappella data were collected to observe the evolution of the active cone and associated lava flow. The Capella constellation includes commercial X-band SAR satellites that provide rapid- and repeated-acquisition of high-resolution imagery for government, commercial and research organizations. This constellation consists of 7 satellites (at the time of writing) orbiting at 3 different inclinations (97°, 53°, 45°) at ~500 km altitude. Each platform includes a SAR antenna coupled with a boom and antenna reflector, capable of acquiring images in various modes (from Stripmap to Spotlight) and incidence angles (15–45°), with left- or right-viewing geometry. This particular setting allows parameters to be adjusted for the target location, image size and spatial resolution, while maintaining daily revisit capability*.

Acquisition was tasked on 30 September, and 3 images were collected on 01, 02 and 04 October 2022 (see Supplementary Material Table S3). Images were in Spotlight mode with the highest spatial resolution (<50 cm/pixel) for a coverage of ~5 × 5 km^2. At single-look-complex (SLC) processing level† these images provide a slant-range view of the ground. SLC images are affected by geometric distortions such as layover, foreshortening or shadowing. These distortions prevent the images from being used to precisely measure the size of the observed objects, but they could be corrected if the topography would be known *a priori*. In the case of relatively flat features such as lava flows, the distortions are minimized and topographically-georeferenced (GEO) images can be used instead. Yet here, SLC images provide a clear view of the ground that allow us to visually track the growth of the eruptive cone.

3.5 Infrared satellite imagery

Infrared satellite imagery was collected for two purposes. One was to extract the lava flow outline and the other to estimate the discharge rate and emitted lava volume, as usually done at Piton de la Fournaise [Coppola et al. 2013; 2016].

Shortwave infrared (SWIR) images were acquired via the Multispectral Instrument (MSI) onboard Copernicus' Sentinel-2 sun-synchronous platforms (Supplementary Material Figure S3). These images have a spatial resolution of 20 m/pixel and a temporal resolution of 5 days over Piton de la Four-

*https://support.capellaspace.com/hc/en-us/article_attachments/18539279613588

†https://support.capellaspace.com/hc/en-us/article_attachments/18539279613588

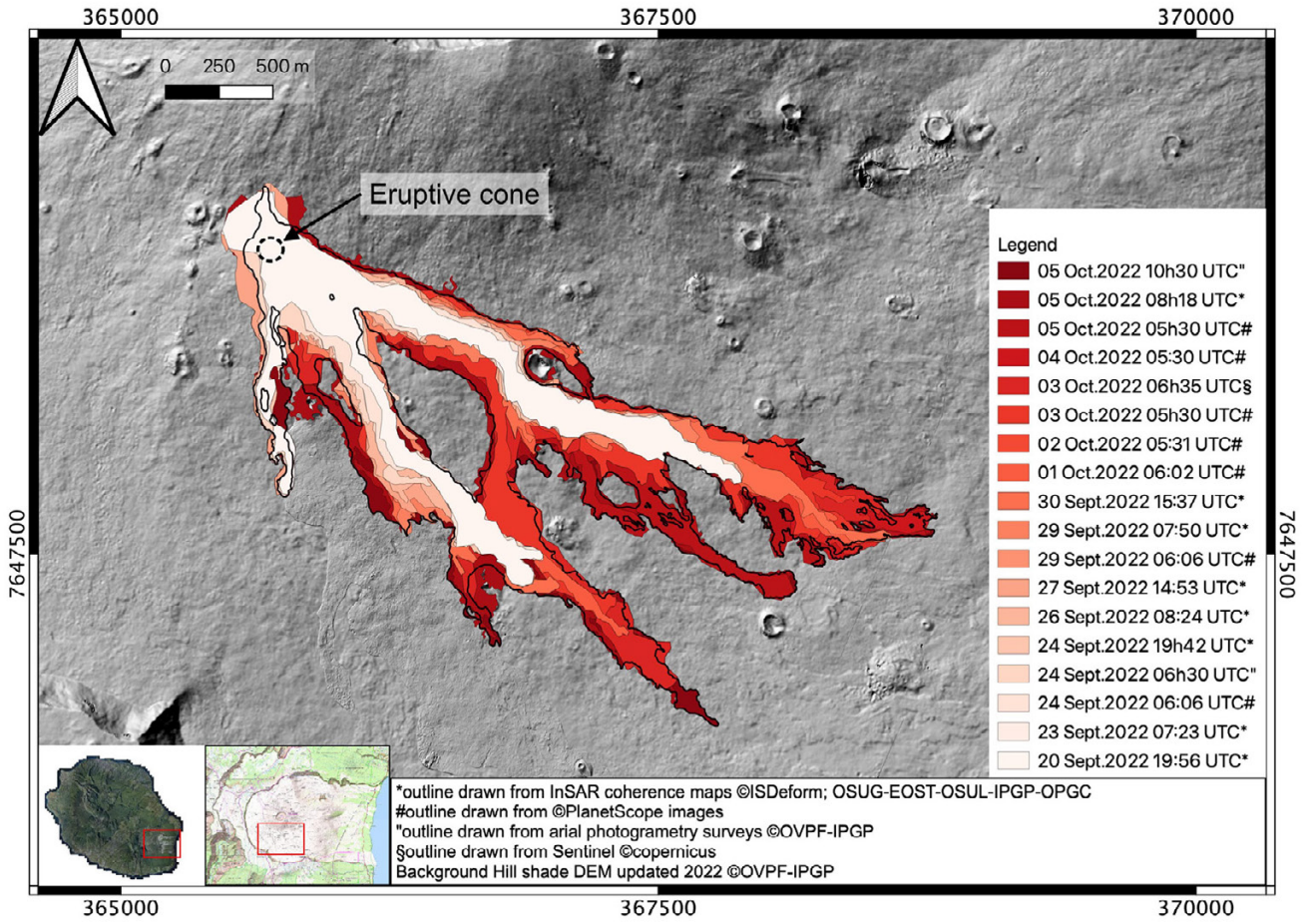

Figure 3: Lava flow field evolution over time obtained through the various techniques. The bold black line indicates the final lava flow outline obtained by aerial SfM photogrammetry on 05 October. Coordinates are in meters within system WGS84-UTM 40S.

naise. The images were analyzed considering the Level 1C top-of-atmosphere SWIR reflectance in the ρ12 (2.19 µm), ρ11 (1.61 µm), and ρ8A (0.86 µm) bands [Massimetti et al. 2020]. The first image was acquired on 28 September 2022 and showed the lava flow activity on the north flow branch, but the lava outline could not be mapped due to cloud cover. The image acquired on 03 October 2022 at 06:35 UTC showed the full extent of the lava flow and was used to extract a lava flow outline. The last image was acquired on 08 October, after the end of the eruption, and showed remaining areas of hot lava but it was not used to determine the flow outline (Supplementary Material Figure S2).

Middle infrared (MIR) data were acquired with the Moderate Resolution Imaging Spectroradiometer (MODIS) and the Visible Infrared Imaging Radiometer Suite (VIIRS), which together provide about eight images per day (two nighttime and two daytime images per sensor). Both the sensors-retrieved data were processed by the Middle Infrared Observations of Volcanic Activity (MIROVA) system developed at the University of Turin, Italy* [Coppola et al. 2016; Campus et al. 2022]. MIROVA allows the heat radiated by the lava flow to be quantified at the time of the satellite acquisition and to be converted into Time-Averaged Discharge Rate (TADR) [Coppola et al. 2013; 2016] with an uncertainty of ±35% [Harris et al. 2017; Chevrel et al. 2022; Verdurme et al. 2022]. The time series of TADR were manually filtered in order to discard the data contaminated by clouds and/or acquired in bad geometrical conditions. During the 16 days of eruption and thanks to the association of MODIS and VIIRS data, we obtained more than 50 data points. This represents around three points per day, making this eruption one of the most well-covered at Piton de la Fournaise.

In addition, the discharge rate was also obtained from the HOTVOLC platform that uses infrared data provided by the MSG-SEVIRI (Spinning Enhanced Visible and Infrared Imager) sensor [Labazuy et al. 2012; Gouhier et al. 2016; 2022]. This method allows data to be collected every 15 min but with uncertainties of 50%.

The cumulative volume of emitted lava was derived from the estimated discharge rate obtained from MIROVA and HOTVOLC. This method implies volume uncertainties of 35% and 50%, respectively.

4 Results

4.1 Lava flow outline and morphometry

In total 18 lava flow outlines were defined (Table 1 and Figure 3) using images obtained from the various techniques and sensors. The lava flow outlines were mapped almost daily, hence in chronological order. Depending on the data, either

*www.mirovaweb.it

Table 1: Details on the image acquisitions used to produce the daily monitoring of the lava flow outline. Total lava flow area (km^2) and perimeter (km) of the outlines as obtained with QGIS toolbox are also given.

Acquisition method	Date (DD/MM/YY)	Time UTC (HH:MM)	Time after start of eruption (h)	Area (km^2)	Perimeter (km)
Start of the eruption 19/09/22 at 03:48 UTC					
InSAR	20/09/22	19:56	40	0.66	12.14
InSAR	23/09/22	07:23	100	0.71	12.09
PlanetScope	24/09/22	06:06	122	0.68	11.69
SfM	24/09/22	06:30	123	0.70	13.49
InSAR	24/09/22	19:42	136	0.69	11.72
InSAR	26/09/22	08:24	173	0.82	12.55
InSAR	27/09/22	14:53	203	0.93	12.93
PlanetScope	29/09/22	06:06	242	0.86	12.69
InSAR	29/09/22	07:50	244	0.96	13.49
InSAR	30/09/22	15:37	276	1.03	16.41
PlanetScope	01/10/22	06:02	290	1.09	17.42
PlanetScope	02/10/22	05:31	314	1.23	19.01
PlanetScope	03/10/22	05:30	338	1.34	19.55
Sentinel2 RGB	03/10/22	06:35	339	1.52	19.84
PlanetScope	04/10/22	05:30	363	1.56	20.13
PlanetScope	05/10/22	05:30	387	1.75	24.07
InSAR	05/10/22	08:18	389	1.93	32.34
SfM	05/10/22	10:30	392	1.90	31.81
End of the eruption 05/10/22 at 06:10 UTC					

the entire flow field was visible (aerial orthomosaics and InSAR coherence maps) or in the case of PlanetScope images only the active parts of the flow were well visible (Figure 2). For this reason, the outline of day D was obtained from the outline of day D-1. If a part of the flow was not visible anymore on D but was present on D-1, it was kept. This allowed the flow field area to continually grow by implementation and to avoid misinterpretation by missing parts of the flow field. The only exceptions are the 2 outlines acquired from airborne surveys on 24 September and 5 October and the last outline obtained from the InSAR coherence map on 05 October. In these cases, the outlines were defined without prior knowledge of the flow field and allowed an independent validation of the covered area.

Lava flow area and perimeter were extracted using the QGIS toolbox on the reference DSM (Figure 3). Results show that over the first day of the eruption (first outline obtained on 20 September at 19:56 UTC, 40 h after the eruption onset) the lava flow field had quickly developed 3 branches: a short branch to the south parallel to the fissure extension and reaching a distance of 1 km, and two larger branches flowing toward the east. The northern branch was the longest and had reached a distance of 2.5 km, while the other branches reached distances of 2.0 km (Figures 3 and 4). On 20 September, the flow field had covered an area of 0.66 km^2, at a rate of 0.4 $km^2\ d^{-1}$. Over the next 10 days the lava flow field did not extend significantly but slightly widened at a rate of 0.02 $km^2\ d^{-1}$ (Figure 4).

The increase in activity observed during the night of 29 September was marked by a significant change in the flow field geometry. On 30 September, the north main branch had lengthened by 750 m and on 01 October the south branch by 470 m. On 02 October, the lava from the north branch broke out, forming a new flow branch that reached the southern branch. On 04 October another breakout formed a new branch, parallel to the others and reaching a distance of 1 km. Over these days and until the end of the eruption (29 September to 05 October) the flow field grew at a rate of 0.2 $km^2\ d^{-1}$. By the end of the eruption, on 05 October, the lava flow had reached a maximum distance from the vent of 3.3 km and covered an area of 2 km^2 (Table 1). We note that the perimeter of the lava flow followed a similar increasing trend as the area, except for the two final data acquisitions obtained from InSAR and SfM, that have much higher values (Table 1 and Figure 4). These higher values are due to the more precise and sinuous outlines rather than a significant lava addition (as revealed by a smaller lava flow area increase).

The final covered area as outlined by SfM analyses is 1.9 km^2. Considering this surface and the errors of the DSMs, the final volume was estimated at 11.6 km^3 with an uncertainty of 0.5 km^3 based on model errors. The final flow thickness reached up to 25 m (see map in Supplementary Material Figure S1).

4.2 Eruptive cone morphology

Important changes in the eruptive cone morphology during the eruption are documented by the four DSM obtained from the SfM photogrammetry and by three Capella images (Figure 5).

After the first day of the eruption, the lava source focused on a single vent, as often observed in similar basaltic effusive

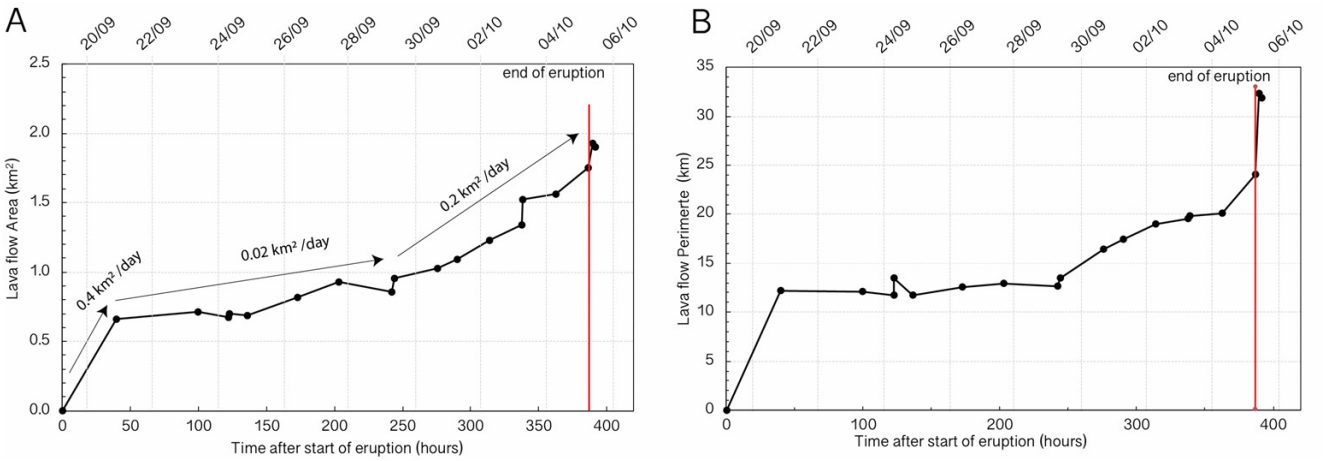

Figure 4: [A] Cumulative area and [B] perimeter of the lava flow field calculated from the mapping.

eruptions [Jones and Llewellin 2021]. On 24 September, a scoria cone at the main vent had reached 18 m in height, 72 m at the base, and had a crater size of 28 m. A smaller lateral cone of a few meters high was still active to the south (Figure 5A). Four days later, on 28 September, the main cone had grown by a few meters (25 m high and 76 m wide) and narrowed at the top, almost closing up, with a crater size of 8 m. The lateral cone did not change significantly (Figure 5B).

The increase in activity observed on 29 September was accompanied by strong lava fountaining. This higher material supply rate contributed to significant growth and enlargement of the scoria cone. On the Capella images acquired on 01, 02 and 04 October, we observed a well-developed cone with a large circular crater and no evidence of lateral collapse (Figure 5E–G). The growth of the cone embraced and covered the lateral vent. With the DSM obtained on 03 October, we measured more precisely the crater diameter to 74 m while the cone had grown to 36 m high and doubled its base diameter to 142 m (Figure 5C). Two days later, when the eruption ended, the final scoria cone was 41 m high with a base of 158 m and a crater diameter of 81 m, similar to its neighbor (Figure 5D) with only a small scar on the main cone remaining from the lateral vent. The new volcanic cone was named *Piton Tikal**.

4.3 TADR and derived volume

The satellite-retrieved TADR time series shows a well-known pattern of Piton de la Fournaise eruptions with an exponential decrease over the first days and an increase near the end of the eruption [Coppola et al. 2016; Campus et al. 2022]. This trend is characterized by 4 main phases: i) an initial (19 September) TADR peaking at about $30\,m^3\,s^{-1}$ (maximum value is measured by HOTVOLC) that sharply declined to less than $5\,m^3\,s^{-1}$ in 24 h; ii) an intermediate (20–29 September) phase lasting about 9–10 days in which the TADR remained almost stable at 2–5 $m^3\,s^{-1}$; iii) a third phase (29 September–02 October) characterized by a gradual increase of TADR up to a maximum of $25\,m^3\,s^{-1}$ as measured by MIROVA and $33\,m^3\,s^{-1}$ by HOTVOLC, and iv) final phase (02–05 October) of high flux around $14\,m^3\,s^{-1}$ on average as measured by MIROVA ($9\,m^3\,s^{-1}$ on average as measured by HOTVOLC) that suddenly stopped on 5 October 2022.

Cumulated lava flow volume is estimated by integration of the flow rate over time and ranges from about $8 \pm 4\,Mm^3$ as obtained from HOTVOLC to $11 \pm 3\,Mm^3$ as obtained via MIROVA (Figure 6). This last volume estimate compares very well with the volume calculated from the acquired local DSM ($11.6 \pm 0.5\,Mm^3$).

5 Interpretation and Discussion

5.1 Lava flow field evolution

Lava flow length is prominently controlled by lava effusion rate [Harris et al. 2007]. Here we observed that the lava flow growth follows the fluctuation of the estimated TADR. Over the first 2 days of the eruption, when the effusion rate was high, the lava flow quickly extended up to 2.5 km long. During this first phase the lava emplacement was dominated by channel-fed flow with a dispersed flow front advancing as rubbly ʻaʻā at a rate of $50\,m\,h^{-1}$ and $0.4\,km^2\,d^{-1}$. During the second phase between 20 to 29 September, when the effusion rate was low and steady ($2–5\,m^3\,s^{-1}$), the lava flow did not extend further. Instead, the flow fronts remained inactive while the proximal area slowly widened and thickened through multiple pāhoehoe breakouts fed by lava tube architecture as evidenced by PlanetScope images (Figure 7A–C, see also Figure 1C). At such low effusion rate the lava is not able to stay hot and fluid to travel far enough to extend the flow. Instead, lava is transported in the subsurface (through non-mature tube systems) and dominated by short and punctual ephemeral breakouts of pāhoehoe lava. Such breakouts feed small channels that extend no more than a few hundred meters from the eruptive vent (Figure 7A). The cooling-limited length of these breakouts is reached quickly due to the low effusion rate.

After 29 September, the increased effusion rate allowed the lava flow field to extend further. The higher effusion

*The name *Piton Tikal* was chosen because the cone strongly resembles its neighbor *Piton Kalla et Pellé*. These names refer to the tales and legends of La Réunion associated with *Gran Mèr Kal* (Grandmother Kal) an old lady who lives in the volcano. In various of these *zistwar* (tales) reference is sometimes made to her son, under the name of *Ti Kala* or *Tikal* (that could be translated to Kal Junior).

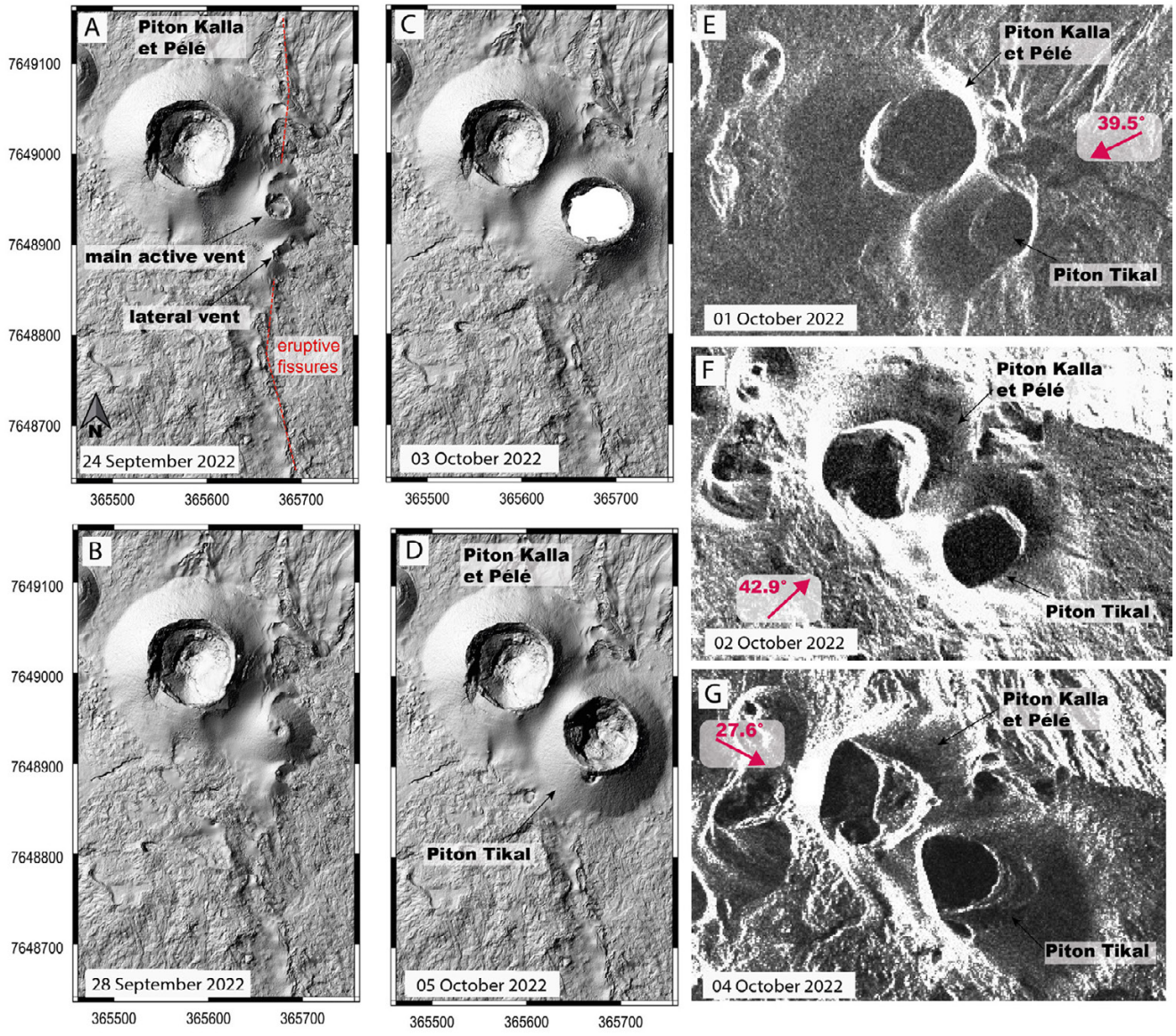

Figure 5: Evolution of the eruptive cone morphology. [A–D] Hillshade DSM (north toward the top) showing the eruptive vent (named *Piton Tikal* at the end of the eruption) growing to the east of an old cone *Piton Kalla et Pélé*. Images were obtained by aerial SfM photogrammetry taken via ULM on 24 September and 5 October and via UAS on 28 September and 3 October. On the image of 03 October, topography inside the crater of *Piton Tikal* could not be obtained. [E–G] Capella SAR images taken on 01, 02 and 04 October. These images are SLC images containing geometrical distortions. Viewing direction and incidence angle with respect to vertical are indicated by the pink arrow. Images are rotated north-up to facilitate interpretation. They are roughly at the same scale as the DSM. The dates of acquisition are indicated on the images.

rate observed from 29 September to the end of the eruption (9–14 $m^3 s^{-1}$) permitted the lava to be transported to the front. Flow fronts were reactivated as observed on the PlanetScope image of 01 October (Figure 7D). The length of the longest branch reached its maximum on 04 October at 3.4 km from the eruptive vent. On 2 occasions (02 and 04 October) we observed well-defined new open channels at the exit of a tube that formed new branches and extended the lava hundreds of meters further (Figure 7E and F).

This daily monitoring allowed us to observe a new breakout to the north on 01 October. The lava flowed around an older scoria cone and threatened a monitoring station located nearby (Figure 7D). As a precaution, the removable parts of the monitoring station were dismantled. The final lava flow contour revealed that the lava had completely surrounded the station and was only 25 m from it. Fortunately, the eruption stopped in time and the station site remained intact.

5.2 Potential of multi-sensors and techniques

During effusive eruptions, lava flow emplacement mapping strategy includes acquiring data at high spatial and temporal resolution and mitigating the lack of visual observations (either from the ground or from space) in periods of adverse meteorological conditions. During this eruption, daily monitoring was

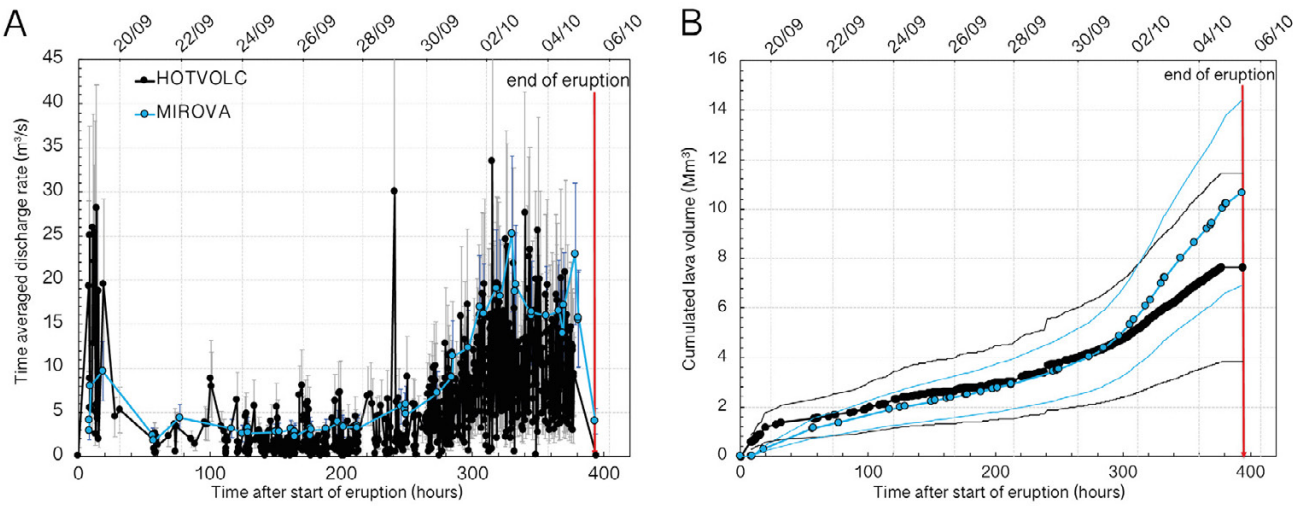

Figure 6: Evolution of [A] time-averaged discharge rates and [B] cumulative volume estimated from the MIROVA (in blue) and HOTVOLC (in black) platforms as a function of time (hours). Dates (DD/MM) are indicated at the top.

achieved thanks to the combination of different sensors and techniques. While aerial SfM photogrammetry and InSAR are typical acquisition techniques at Piton de la Fournaise [Derrien 2019; Harris et al. 2019], this is the first time that PlanetScope data were acquired for this volcano. This new data acquisition was a significant addition to the monitoring as it provided images at a higher rate and hence allowed the daily monitoring of the lava flow growth. PlanetScope images—filtering through NDVI and RTVI indexes—proved to be suitable for lava flow monitoring as they exhibit clear contrasts where active lava emits in the near-infrared. Using these images instead of RGB false-color images was found to be better for visual definition of the lava flow borders and for unravelling lava flow emplacement dynamics (Figure 7). Additionally, the high temporal resolution (1-day revisit) and enhanced spatial resolution (3 m in NIR) of PlanetScope data were proven here to be beneficial in the case of a rapidly evolving lava flow and low cloud cover. This is nonetheless at the expense of spectral resolution with seven visible bands and only one band extending slightly in the IR domain. Alternatively, spectral combinations incorporating shortwave infrared (SWIR) such as Sentinel-2 satellites may be better designed [Massimetti et al. 2020]. However, these are of lower spatial resolution (20 m in the SWIR domain) and lower temporal resolution (5 days revisit). Here, only three Sentinel-2 images were acquired during the time of the eruption and only one (03 October at 06:35 UTC) was found adequate for defining the lava flow outline.

The daily monitoring was especially complete for this eruption because of the combination of several techniques but also because of the low cloud cover from the fifth day of the eruption. Yet, due to its location in an insular tropical context and its topography, Piton de la Fournaise is often affected by bad weather conditions. For this reason, radar sensors are very useful as they penetrate the clouds. During this eruption, the first two ALOS-2 radar images collected on 20 and 23 September 2022 were hence particularly important as the weather was bad and no other visual direct observation of the eruption had been possible at that time. Despite its performance even in cloudy conditions, InSAR data alone cannot be used for daily monitoring of lava flows. Indeed, considering both S1 and Spotlight ALOS-2 images, the acquisition recurrence time is on average 1 image every 2 days. We must also consider the delay between image acquisition, data availability, and processing that is in part automated but often requires the intervention of a human operator. Together, the delay between image acquisition and delivery to OVPF-IPGP is estimated at between 48 to 72 hours, which is not ideal for rapid evolving lava propagation and a real-time response to a volcano crisis.

During the eruption, we also acquired radar Capella products for the first time at Piton de la Fournaise. Images were acquired in "daily revisit" tasking mode and delivered between 2.5 and 7.5 hours after collection. This short revisit time provided limited stability of geometric parameters. Unlike S1 data, all Capella images are acquired with different viewing angles, which precludes detailed day-to-day comparisons between the images (and, by extension, makes one-day interferometry unfeasible). All 3 images acquired on 01, 02 and 04 October were acquired with substantially different incidence angles preventing the application of standard change detection methods (Figure 5). Furthermore, due to the oblique-looking viewing geometry of the radar, the limited resolution of the DSM used for the radar image geocoding, combined with an evolving topography (due to eruptive cone growth, lava flow accumulation, etc.) led to substantial residual geometric distortions at small scale even after correction (GEO products). This imposes the use of SLC products, which correspond to the native geometry of SAR, but cannot be used for quantitative measurements and requires interpretation by a radar expert. The Capella images can nevertheless be used to track the growth of the eruptive cone (Figure 5). In general such images are therefore ideal for monitoring vent morphology during eruptions as they have high spatial and temporal reso-

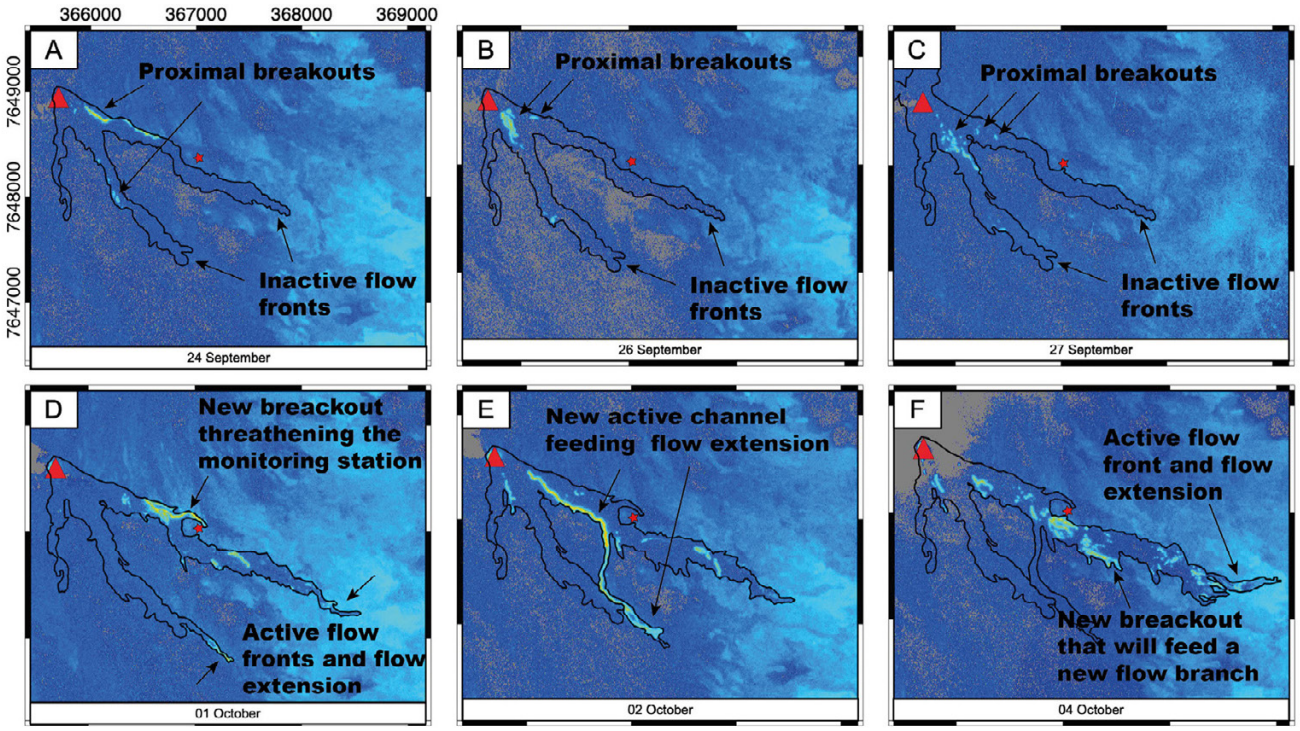

Figure 7: Images from PlanetScope filtered with red edge triangular vegetation index (RTVI) showing the active parts of the flow through emplacement over the eruption. The red triangle represents the main vent. The red star indicates the location of the monitoring station. Indices color scale (cold to warm) reflect thermal radiation intensity emitted by active lava flow. [A–C] are acquired during the phase of low effusion rate between 20 to 29 September while [D–F] are acquired during the phase of higher effusion rate between 29 September to 05 October.

lution and are insensitive to cloud cover and to the gas plume [e.g. Ezquerro et al. 2023].

6 Conclusion

The dataset presented here was assembled thanks to collective work using a large variety of sensors and techniques from various institutes. Satellite radar imagery was of primary importance to validate the extent of the lava flow under cloudy conditions over the first days of the eruption. When the weather became cloud-free, the PlanetScope imagery provided an exceptional dataset allowing us to track the lava flow at high temporal and spatial resolution (daily overpass). Over the 16 days of the eruption, we obtained 18 lava flow outlines with up to 3 outlines per day.

Thanks to the daily mapping, we observed in detail how the restart in activity that occurred on 29 September was accompanied by a significant advance of the existing flow branches, an increase in the complexity of the flow field and a modification of the cone morphology. It also allowed us to anticipate the trajectory of the lava flow and salvage a monitoring station that was potentially at risk. The presented data set also provides material for a deeper study of the lava flow activity highlighting the active parts of the flow with high precision. Further correlation with TADR, lava flow growth (shape and size) as well as tremor activity could also be conducted and serve as a benchmark for numerical simulations of lava flow propagation.

Such a daily follow-up is therefore important for the volcano observatory as well as for the local authorities, especially in the event of eruptions that would threaten infrastructure, properties and people. This coordinated effort in providing data from several institutes and using various techniques should be carried on for future eruptions at Piton de La Fournaise and, where feasible, may serve as an example to be transposed to other active volcanic sites.

Author Contributions

MOC gathered the data and led this study. MOC, NV, JLF drew the lava flow outline. NV performed the aerial survey and photogrammetry. DC, FM, AC processed the MIROVA data. RG processed and provided the PlanetScope© SuperDove and Capella© products. JLF processed and provided the InSAR images. All authors contributed to implementing and writing of the report.

Acknowledgements

We warmly acknowledge the entire OVPF-IPGP staff that scrupulously monitors the eruptions at Piton de la Fournaise, and the *Section aérienne de la gendarmerie* (SAG) for providing helicopter support. The authors thank the Kalidéos program and ESA for kindly providing the Pléiades triplet in the frame of a collaboration agreement. The authors are also grateful with the webservice of ForM@Ter, Solid Earth component of the Data Terra Research Infrastructure team, without whom the calculation of DSM would have been im-

possible. ©PlanetScope SuperDove products are copyright of Planet company, provided by R. Grandin (IPGP) under "Education and Research Standard License n°81527". ©Capella imagery is copyright of the ©Capella company, provided by R. Grandin (IPGP). The ALOS-2 data were provided by the Japanese Aerospace Exploration Agency (JAXA) under the 3rd Research Announcement on the Earth Observation (EO-RA3). OI2 is a component of the French CNRS-INSU National Observation Service ISDeform. HOTVOLC data were supported by French CNRS-INSU through SNOV, and by French Space Agency the Centre National d'Etudes Spatiales (CNES). AH acknowledge iCRAG—the Science Foundation Ireland Research Centre in Applied Geosciences—and European Space Agency Living Planet Fellowship for their funding, (iCRAG-Phase 2 – Grant Code: 13/RC/2092_P2 and Grant Code: 73738). This is Laboratory of Excellence ClerVolc contribution n° 610.

Data Availability

Most of the data presented here have been published in OVPF-IPGP bulletins and reports (ISSN 2610-5101) and are available at https://www.ipgp.fr/communiques-et-bulletins-de-lobservatoire/. All data presented here are available upon request to the corresponding author and to the OVPF-IPGP. Access to @Capella SAR images and @Planet optical images is subject to license agreement, which can be requested from the @Capella and @Planet companies. All InSAR products stored within OI2 are available at https://wwwobs.univ-bpclermont.fr/casoar/resources/php/Accounts/login.php.

Copyright notice

References

Bachèlery, P. (1981). "Le Piton de la Fournaise (Ile de La Réunion). Etude volcanologique, structural et pétrologique". PhD thesis. Université Clermont-Ferrand II.

Bato, M., J. Froger, A. Harris, and N. Villeneuve (2016). "Monitoring an effusive eruption at Piton de la Fournaise using radar and thermal infrared remote sensing data: insights into the October 2010 eruption and its lava flows". *Geological Society, London, Special Publications* 426, pages 533–552. DOI: 10.1144/SP426.30.

Campus, A., M. Laiolo, F. Massimetti, and D. Coppola (2022). "The transition from MODIS to VIIRS for global volcano thermal monitoring". *Sensors* 22(5), page 1713. DOI: 10.3390/s22051713.

Chen, P.-F., T. Nicolas, J.-H. Wang, V. Philippe, W.-J. Huang, B.-G. Li, et al. (2010). "New index for crop canopy fresh biomass estimation". *Spectroscopy and Spectral Analysis* 30(2), pages 512–517. DOI: 10.3964/j.issn.1000-0593(2010)02-0512-06.

Chevrel, M. O., M. Favalli, N. Villeneuve, A. J. Harris, A. Fornaciai, N. Richter, A. Derrien, P. Boissier, A. Di Muro, and A. Peltier (2021). "Lava flow hazard map of Piton de la Fournaise volcano". *Natural Hazards and Earth System Sciences* 21(8), pages 2355–2377. DOI: 10.5194/nhess-21-2355-2021.

Chevrel, M. O., A. Harris, A. Peltier, N. Villeneuve, D. Coppola, M. Gouhier, and S. Drenne (2022). "Volcanic crisis management supported by near real-time lava flow hazard assessment at Piton de la Fournaise, La Réunion". *Volcanica* 5(2), pages 313–334. DOI: 10.30909/vol.05.02.313334.

Coppola, D., M. Laiolo, C. Cigolini, D. D. Donne, and M. Ripepe (2016). "Enhanced volcanic hot-spot detection using MODIS IR data: results from the MIROVA system". *Geological Society, London, Special Publications* 426, pages 181–205. DOI: 10.1144/SP426.5.

Coppola, D., M. Laiolo, D. Piscopo, and C. Cigolini (2013). "Rheological control on the radiant density of active lava flows and domes". *Journal of Volcanology and Geothermal Research* 249, pages 39–48. DOI: 10.1016/j.jvolgeores.2012.09.005.

Derrien, A. (2019). "Apports des techniques photogrammétriques à l'étude du dynamisme des structures volcaniques du piton de la fournaise". PhD thesis. Université Paris Cité.

Derrien, A., A. Peltier, N. Villeneuve, and T. Staudacher (2020). "The 2007 caldera collapse at Piton de la Fournaise: new insights from multi-temporal structure-from-motion". *Volcanica* 3(1), pages 55–65. DOI: 10.30909/vol.03.01.5565.

Derrien, A., N. Villeneuve, A. Peltier, and L. Michon (2019). "Multi-temporal airborne structure-from-motion on caldera rim: Hazard, visitor exposure and origins of instabilities at Piton de la Fournaise". *Progress in Physical Geography: Earth and Environment* 43(2), pages 193–214. DOI: 10.1177/0309133318808201.

Dietterich, H. R., M. P. Poland, D. A. Schmidt, K. V. Cashman, D. R. Sherrod, and A. T. Espinosa (2012). "Tracking lava flow emplacement on the east rift zone of Kilauea, Hawai 'i, with synthetic aperture radar coherence". *Geochemistry, Geophysics, Geosystems* 13(5). DOI: 10.1029/2011GC004016.

Ezquerro, P., G. Bru, I. Galindo, O. Monserrat, J. García-Davalillo, N. Sánchez, I. Montoya, R. Palamà, R. Mateos, R. Pérez-López, et al. (2023). "Analysis of SAR-derived products to support emergency management during volcanic crisis: La Palma case study". *Remote Sensing of Environment* 295, page 113668. DOI: 10.1016/j.rse.2023.113668.

Got, J.-L., A. Peltier, T. Staudacher, P. Kowalski, and P. Boissier (2013). "Edifice strength and magma transfer modulation at Piton de la Fournaise volcano". *Journal of Geophysical Research: Solid Earth* 118(9), pages 5040–5057. DOI: 10.1002/jgrb.50350.

Gouhier, M., Y. Guéhenneux, P. Labazuy, P. Cacault, J. Decriem, and S. Rivet (2016). "HOTVOLC: A web-based monitoring system for volcanic hot spots". *Geological Society, London, Special Publications* 426(1), pages 223–241. DOI: 10.1144/SP426.31.

Gouhier, M., V. Pinel, J. Belart, M. De Michele, C. Proy, C. Tinel, E. Berthier, Y. Guéhenneux, M. T. Gudmundsson, B. V. Óskarsson, et al. (2022). "CNES-ESA satellite contribution to the operational monitoring of volcanic activity: The 2021 Icelandic eruption of Mt. Fagradalsfjall". *Journal of Applied Volcanology* 11(1), pages 1–16. DOI: 10.1186/s13617-022-00120-3.

Harris, A. J., M. O. Chevrel, D. Coppola, M. Ramsey, A. Hrysiewicz, S. Thivet, N. Villeneuve, M. Favalli, A. Peltier, P. Kowalski, et al. (2019). "Validation of an integrated satellite-data-driven response to an effusive crisis: the April–May 2018 eruption of Piton de la Fournaise". *Annals of Geophysics* 61(2018)). DOI: 10.4401/ag-7972.

Harris, A. J., J. Dehn, and S. Calvari (2007). "Lava effusion rate definition and measurement: a review". *Bulletin of Volcanology* 70, pages 1–22. DOI: 10.1007/s00445-007-0120-y.

Harris, A. J., N. Villeneuve, A. Di Muro, V. Ferrazzini, A. Peltier, D. Coppola, M. Favalli, P. Bachèlery, J.-L. Froger, L. Gurioli, et al. (2017). "Effusive crises at Piton de la Fournaise 2014–2015: a review of a multi-national response model". *Journal of Applied Volcanology* 6(1), pages 1–29. DOI: 10.1186/s13617-017-0062-9.

Hrysiewicz, A. (2019). "Caractérisation des déplacements liés aux coulées de lave au Piton de la Fournaise à partir de données InSAR". PhD thesis. Université Clermont Auvergne.

James, M. R., B. Carr, F. D'Arcy, A. Diefenbach, H. Dietterich, A. Fornaciai, E. Lev, E. Liu, D. Pieri, M. Rodgers, et al. (2020). "Volcanological applications of unoccupied aircraft systems (UAS): Developments, strategies, and future challenges". *Volcanica* 3(1), pages 67–114. DOI: 10.30909/vol.03.01.67114.

Jones, T. J. and E. W. Llewellin (2021). "Convective tipping point initiates localization of basaltic fissure eruptions". *Earth and Planetary Science Letters* 553, page 116637. DOI: 10.1016/j.epsl.2020.116637.

Labazuy, P., M. Gouhier, A. Harris, Y. Guéhenneux, M. Hervo, J.-C. Bergès, P. Fréville, P. Cacault, and S. Rivet (2012). "Near real-time monitoring of the April–May 2010 Eyjafjallajökull ash cloud: an example of a web-based, satellite data-driven, reporting system". *International Journal of Environment and Pollution* 48(1-4), pages 262–272. DOI: 10.1504/IJEP.2012.049673.

Massimetti, F., D. Coppola, M. Laiolo, S. Valade, C. Cigolini, and M. Ripepe (2020). "Volcanic hot-spot detection using SENTINEL-2: a comparison with MODIS–MIROVA thermal data series". *Remote Sensing* 12(5), page 820. DOI: 10.3390/rs12050820.

Massonnet, D. and K. L. Feigl (1998). "Radar interferometry and its application to changes in the Earth's surface". *Reviews of Geophysics* 36(4), pages 441–500.

Michon, L., A. Di Muro, N. Villeneuve, C. Saint-Marc, P. Fadda, and F. Manta (2013). "Explosive activity of the summit cone of Piton de la Fournaise volcano (La Réunion island): a historical and geological review". *Journal of Volcanology and Geothermal Research* 264, pages 117–133. DOI: 10.1016/j.jvolgeores.2013.06.012.

OVPF (2022). *Monthly bulletin of the Piton de la Fournaise Volcanological Observatory—September 2022*. Technical report, ISSN 2610–5101. DOI: 10.18715/REUNION.OVPF.

Peltier, A., P. Bachèlery, and T. Staudacher (2009). "Magma transport and storage at Piton de La Fournaise (La Réunion) between 1972 and 2007: A review of geophysical and geochemical data". *Journal of Volcanology and Geothermal Research* 184(1-2), pages 93–108. DOI: 10.1016/j.jvolgeores.2008.12.008.

Peltier, A., M. O. Chevrel, A. J. Harris, and N. Villeneuve (2022). "Reappraisal of gap analysis for effusive crises at Piton de la Fournaise". *Journal of Applied Volcanology* 11(1), pages 1–17. DOI: 10.1186/s13617-021-00111-w.

Peltier, A., V. Ferrazzini, A. Di Muro, P. Kowalski, N. Villeneuve, N. Richter, O. Chevrel, J. L. Froger, A. Hrysiewicz, M. Gouhier, D. Coppola, L. Retailleau, F. Beauducel, L. Gurioli, P. Boissier, C. Brunet, P. Catherine, F. Fontaine, F. Lauret, L. Garavaglia, J. Lebreton, K. Canjamale, N. Desfete, C. Griot, A. Harris, S. Arellano, M. Liuzzo, S. Gurrieri, and M. Ramsey (2021). "Volcano Crisis Management at Piton de la Fournaise (La Réunion) during the COVID-19 Lockdown". *Seismological Research Letters* 92(1), pages 38–52. DOI: 10.1785/0220200212.

Peltier, A., N. Villeneuve, V. Ferrazzini, S. Testud, T. Hassen Ali, P. Boissier, and P. Catherine (2018). "Changes in the long-term geophysical eruptive precursors at Piton de la Fournaise: Implications for the response management". *Frontiers in Earth Science* 6, page 104. DOI: 10.3389/feart.2018.00104.

Poland, M. P. (2022). "Synthetic aperture radar volcanic flow maps (SAR VFMs): A simple method for rapid identification and mapping of volcanic mass flows". *Bulletin of Volcanology* 84(3), page 32. DOI: 10.1007/s00445-022-01539-7.

Richter, N. and J.-L. Froger (2020). "The role of Interferometric Synthetic Aperture Radar in detecting, mapping, monitoring, and modelling the volcanic activity of Piton de la Fournaise, La Réunion: A review". *Remote Sensing* 12(6), page 1019. DOI: 10.3390/rs12061019.

Roult, G., A. Peltier, B. Taisne, T. Staudacher, V. Ferrazzini, A. Di Muro, et al. (2012). "A new comprehensive classification of the Piton de la Fournaise activity spanning the 1985–2010 period. Search and analysis of short-term precursors from a broad-band seismological station". *Journal of Volcanology and Geothermal Research* 241-242, pages 78–104. DOI: 10.1016/j.jvolgeores.2012.06.012.

Rouse Jr, J. W., R. H. Haas, D. Deering, J. Schell, and J. C. Harlan (1974). *Monitoring the vernal advancement and retrogradation (green wave effect) of natural vegetation*. Technical report, page 19750020419.

Rupnik, E., M. P. Deseilligny, A. Delorme, and Y. Klinger (2016). "Refined satellite image orientation in the free open-source photogrammetric tools Apero/Micmac". *ISPRS Annals of the Photogrammetry, Remote Sensing and Spatial Information Sciences* III-1, pages 83–90. DOI: 10.5194/isprs-annals-III-1-83-2016.

Rupnik, E., M. Pierrot-Deseilligny, and A. Delorme (2018). "3D reconstruction from multi-view VHR-satellite images in MicMac". *ISPRS Journal of Photogrammetry and Remote Sensing* 139, pages 201–211. DOI: 10.1016/j.isprsjprs.2018.03.016.

Servadio, Z., N. Villeneuve, and P. Bachlery (2012). "Automatic mapping of the lava flows at Piton de la Fournaise volcano, by combining thermal data in near and visible infrared". *Remote Sensing - Applications*. Edited by B. Escalante-Ramirez. IntechOpen, pages 201–220. DOI: 10.5772/37685.

Servadio, Z. (2011). "Apports de l'imagerie à haute résolution spectrale et spatiale dans les bilans de volume et bilans radiatifs au Piton de La Fournaise". PhD thesis. Université de la Réunion.

Staudacher, T., A. Peltier, V. Ferrazzini, A. Di Muro, P. Boissier, P. Catherine, P. Kowalski, F. Lauret, and J. Lebreton (2016). "Fifteen Years of Intense Eruptive Activity (1998–2013) at Piton de la Fournaise Volcano: A Review". *Active Volcanoes of the Southwest Indian Ocean: Piton de la Fournaise and Karthala*. Edited by P. Bachelery, J.-F. Lenat, A. Di Muro, and L. Michon. Berlin, Heidelberg: Springer Berlin Heidelberg, pages 139–170. DOI: 10.1007/978-3-642-31395-0_9.

Tu, Y.-H., K. Johansen, B. Aragon, M. M. El Hajj, and M. F. McCabe (2022). "The radiometric accuracy of the 8-band multispectral surface reflectance from the planet SuperDove constellation". *International Journal of Applied Earth Observation and Geoinformation* 114, page 103035. DOI: 10.1016/j.jag.2022.103035.

Verdurme, P., S. Carn, A. J. Harris, D. Coppola, A. Di Muro, S. Arellano, and L. Gurioli (2022). "Lava Volume from Remote Sensing Data: Comparisons with Reverse Petrological Approaches for Two Types of Effusive Eruption". *Remote Sensing* 14(2), page 323. DOI: 10.3390/rs14020323.

Vlastélic, I., A. Di Muro, P. Bachèlery, L. Gurioli, D. Auclair, and A. Gannoun (2018). "Control of source fertility on the eruptive activity of Piton de la Fournaise volcano, La Réunion". *Scientific reports* 8, page 14478. DOI: 10.1038/s41598-018-32809-0.